Insight into CaMgSi2O6:Eu2+,Mn2+,Dy3+ Nanoprobes: Influence of Chemical Composition and Crystallinity on Persistent Red Luminescence

Céline Rosticher, Bruno Viana, Guillaume Laurent, Patrick Le Griel, Corinne Chanéac

European Journal of Inorganic Chemistry, 22, 3681-3687 (2015)

Insight into CaMgSi2O6:Eu2+,Mn2+,Dy3+ Nanoprobes: Influence of Chemical Composition and Crystallinity on Persistent Red Luminescence

Céline Rosticher,[1] Bruno Viana,[2] Guillaume Laurent,[1] Patrick Le Griel,[1] Corinne Chanéac,*[1]

[1] C. Rosticher, G. Laurent, P. Le Griel, C. Chanéac, Sorbonne Universités, UPMC Univ Paris 06, CNRS, Collège de France, Laboratoire de Chimie de la Matière Condensée de Paris, 11 place Marcelin Berthelot, 75005 Paris, France.

[2] B. Viana, PSL Research University, Chimie ParisTech - CNRS, Institut de Recherche de Chimie Paris, 11 rue Pierre et Marie Curie, 75005 Paris, France

Corresponding author: corinne.chaneac@upmc.fr

Abstract: Optical imaging in which photons are the information source, seems to be a very relevant technique, less expensive and less harmful than more conventional diagnostic methods and suitable, for instance, for sensitive diagnosis capable of detecting cancer at an early stage. We have recently developed inorganic persistent luminescent nanoparticles (PLNPs) as nanoprobes useful for in vivo imaging that can master the difficulties due to the biological environment such as tissue autofluorescence, absorption or photobleaching since they are excited before. In this work, we focus on silicate materials, $CaMgSi_2O_6$, that emit in the red-near infrared range for several hours. In the aim of improving their luminescent properties and the nanoparticles size, we explore a new way of synthesis allowing a suitable yield of particles and we study the influence of the chemical composition and of the crystalline structure on the luminescence intensity. Adjusting Ca/Mg/Si molar ratio and crystallization temperature, very fine nanoparticles of PLNPs have been obtained with an improvement of luminescence and high production yield necessary to promote the emergence of these nanoprobes in the field of optical imaging.

Introduction

At the nanoscale, luminescent solids are suitable for in vivo imaging that implies some problems due to the biological environment, such as the tissues autofluorescence and absorption [1-2]. Therefore we need to develop luminescent probes that emit in the red-near infrared range: in the biological tissues wavelength therapeutic window (600-1350 nm). Indeed, biological tissues absorb a great range of UV and visible light and only a red-near infrared emission can go through the tissues [2-3]. Three main groups of luminescent inorganic nanomaterials are currently reported. Two of them are related to (i) semiconductor nanocrystals with direct or indirect gap or metal nanocrystals [4-5], and (ii) metal clusters [6-8] for which optical properties originate from quantum confinement effect and electronic transitions between occupied d bands and states above the Fermi level. In this paper, we focus on a third group of compounds for which the luminescence originates from the presence of luminescent centers (dopants) in the solid structure [9-12]. In this case, the luminescence closely depends on matrix or ligand-dopant association and can be adjusted to specific applications (telecommunications, biosciences, solar energy conversion) [13]. Such materials are usually prepared using conventional solid state chemistry [14-17]. More recently, promising novel luminescent nanoparticles based on lanthanide or transition metal doped - oxide composition have been synthesized combining sol-gel and hydrothermal syntheses, opening new field of research in the domain of the in vivo optical imaging systems and new imaging tools [18-20]. These materials are more difficult to investigate as one first required to obtain such matrices at the nanometric scale with acceptable intensity of fluorescence [21-23].

A first generation of inorganic luminescent nanoparticles (PLNPs), $Ca_{0.2}Zn_{0.9}Mg_{0.9}Si_2O_6$ doped Eu^{2+}, Mn^{2+}, Dy^{3+}, was developed by Le Masne de Chermont et al. [24]. These new long lasting luminescent nanoparticles were excitable with UV light and emitted during several minutes in the red-near infrared range, therefore avoiding the tissues absorption during the light detection. Indeed PLNPs were excited before the injection in the animal that allows to prevent the tissues autofluorescence and to improve the signal-to-noise ratio. The development of these probes is initially based on the red persistent luminescence of $MgSiO_3$ bulk compound, described by Wang et al. [25] in which the emission corresponds to the Mn^{2+} radiative $^4T_1$–$^6A_1$ transition. More recently a second generation with optimized rare earth cation (RE= Ce, Nd, Dy, Pr, Ho, and Er were evaluated) [26] and a mechanism has been proposed to explain the persistent luminescence of these PLNPs where RE^{3+} and oxygen vacancies appears as electron traps, and Mn^{2+} is the recombination luminescent center (with

emission in the red range at 680 nm) [27]. This allowed the validation of a simpler chemical composition for diopside structure [26, 28]. In these silicate-based families, there are still open questions on the influence of the chemical composition and of the crystalline structure on the persistent luminescence intensity.

In order to obtain nanoprobes, a “soft chemistry” synthesis (sol-gel method and acid catalysis) using molecular precursors in a silica matrix was used [24]. It consists in growing luminescent nanocrystals inside a silica matrix which plays the role of a silica reservoir to obtain a doped silicate and limits the crystal growth during thermal treatment at high temperature, mandatory to crystallize a pyroxene phase. However by this technique probe sizes were still too high for an in vivo imaging application. Furthermore the marked aggregation of particles and their low luminescence intensity represent another important disadvantage for their in vivo application. In the present work, persistent luminescence nanoparticles were synthesized using a sol-gel method inspired by Stöber process. This method enables to obtain silica nanoparticles instead of a silica matrix and thus to have a better control of the crystal growth using these nanoreactors. Core-shell type nanoparticles with a crystalline silicate core and an amorphous silica shell are obtained. Such process implies an efficient step of leaching of particles surface to dissolve the residual silica layer. In the aim of improving the persistent luminescence and studying the chemical composition influence on the persistent luminescence properties, we modified Ca/Mg/Si molar ratio. In addition, to compare our different results, the native $Ca_{0.2}Zn_{0.9}Mg_{0.9}Si_2O_6$ doped Eu^{2+}, Mn^{2+}, Dy^{3+} host is used as reference and RE=Dy is kept for sake of comparison [24].

Results and Discussion

Influence of chemical composition and crystallinity on persistent luminescence. XRD data presented on figure1.a show a strong evolution of crystalline structure from diopside phase for C1M1S2 composition to clinoenstatite phase corresponding to $Mg_2Si_2O_6$ composition with the decrease of Ca/Mg molar ratio. The normalized persistent luminescence spectra at room temperature recorded after switching off the UV excitation (120 sec at 365 nm) exhibit three emission bands for all compounds: at 468, 600 and 670 nm (figure 1.b). The band at 468 nm is attributed to the allowed $4f^65d^1 \rightarrow 4f^7$ transition of Eu^{2+}, whereas the bands at 600 and 670 nm correspond to the transition of Mn^{2+} in Ca^{2+} and Mg^{2+} sites respectively. No characteristic Dy^{3+} emission has been observed. At low temperatures (>300K) as reported

elsewhere Eu2+ emission can also be observed but the persistent luminescence occurs from the Mn2+ center which is at room temperature the recombination center.

With the increase of Ca/Mg molar ratio, considering a calibrated measurement with the same amount of compound, luminescence intensity of the three bands decreases and the relative intensities of the two bands at 600 nm and at 670 nm are inversed for lower calcium content. Variation in Ca/Mg molar ratio has therefore an influence both on crystalline structure of particles and on Mn2+ distribution in the two cationic sites. Consequently, the persistent luminescence intensity is enhanced when promoting the emission band at 670 nm observed for the lowest calcium content. Concerning the influence of crystalline structure, such silicate compounds belong to the pyroxenes group for which the general formula is M2M1(SiO3)2, with the small cation M1 surrounded by 6 oxygen atoms and the larger M2 surrounded by 8 oxygen atoms. Small ions, like Mg2+, Fe2+ or Zn2+ always occupy M1 sites while larger ions like Ca2+ or Na+, and rare earth necessarily occupy M2 cationic sites [29, 30]. CaMgSi2O6 composition follows the general structure of the diopside with a monoclinic symmetry. When small ions are the only ions in the matrix, they also occupy M2 site and form an orthopyroxene phase (enstatite Mg2Si2O6) exhibiting an orthorhombic symmetry. In figure 1.a, the phase modification from diopside to enstatite is clearly detected from a calcium substoichiometry greater than 20 percent. Below this calcium content, clinoenstatite remains the main crystalline phase. In previous study enstatite has been reported to be more efficient than diopside structure for optimized luminescent properties in the case of dysprosium doping [26]. Indeed, dysprosium in enstatite acts as a better electron trap according to the conduction band position between diopside and enstatite structures compared to depth of electron trap related to dysprosium. The crystallization of low calcium silicate composition into enstatite structure then leads to an improved LLP according to figure1.b.

In such crystalline structures, as the ionic radius of Mn2+ (in six-fold coordination) is 0.83 Å whereas the radii of Mg2+ and Ca2+ are 0.72 Å and 1.00 Å respectively [31], Ca2+ ions can occupy only the M2 sites while Mg2+ and Mn2+ cations are distributed in both sites, M1 and M2, as demonstrated by optical spectroscopy [32]. Therefore, the decrease in the amount of calcium contributes to vary the host cationic sites for Mn2+ in the crystalline structure. The persistent luminescence spectra clearly show that the quantity of Mn2+ luminescent centers in Mg2+ sites increases with the decrease of Ca/Mg molar ratio according to the relative intensities of Mn(Ca) and Mn(Mg) at 600 nm and 670 nm respectively (figure 1b).

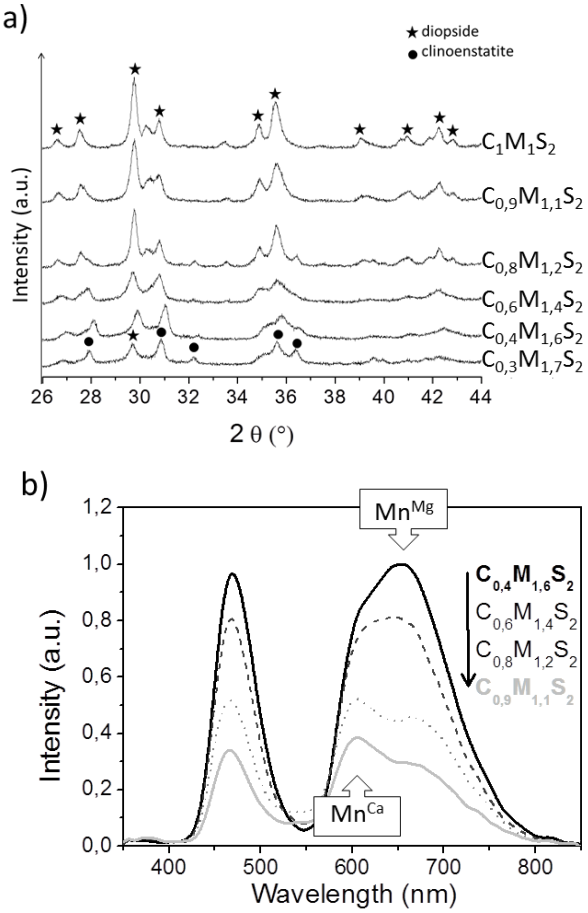

Figure 1. (a) XRD patterns and (b) LLP spectra of CxMyS2O6: Eu0.5% Mn2.5% Dy1% samples corresponding to series A

The substitution of Mg2+ ions by Mn2+ ions inside M1 sites is statically favorable when Mg2+ ions are also distributed into M2 sites. As Mn2+ in Mg2+ site is the luminescent recombination center in the persistent luminescence mechanism; regarding CaMgSi2O6 type of compounds [33], an enhancement of the red afterglow is obtained for Ca0.3Mg1.7Si2O6 composition. Nevertheless, Ca2+ inside the structure is required since a drastic decrease of LLP is observed for Mg2Si2O6 composition, probably related to a high band gap modification. Indeed, the shift of the bottom of the conduction band has been recently reported for Al doped ZnGaO4 phosphors [34].

Interestingly, the LLP also increases with the doping rate without modification of Mn2+ site distribution as shown on LLP decay curves of Ca0.6Mg1.4Si2O6 sample for two different

doping rate, namely Eu(0.5%), Mn(2.5%), Dy(1%) called “doped C1” and Eu1% Mn5% Dy2% called “doped C2” on figure 2.a.

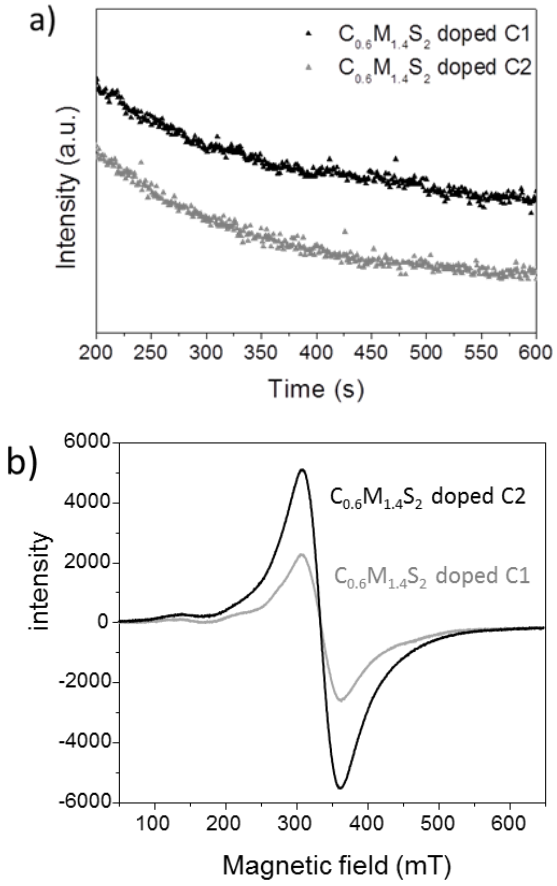

Figure 2. (a) Persistent luminescence decay curves (λ_{exc} = 365 nm, t_{exc} = 120s) and (b) EPR spectra of Ca0.6Mg1.4Si2O6 doped C1 and doped C2.

The loss of persistent luminescence yield versus time appears less important for higher doping rate, and this leads to a significant intensity difference after one-hour term. EPR results (figure 2.b) confirmed that Mn2+ content is two times increased from doped C1 to doped C2 samples. EPR spectra exhibit a fine structure in the central part corresponding to well-ordered Mn2+ and a weaker structure in the wings [31] characteristic of Mn2+ cations in interaction. For the two doping rates, the shape of the spectra is similar indicating that the Mn2+ distribution in crystalline structure is the same and there is no evidence of aggregate for highest content.

The influence of initial concentration of TEOS was then investigated for low Ca/Mg ratio and for both pyroxene based stoichiometric silica content (C0.4M1.6S2) and with an excess in silica content (C0.4M1.6S4). When the initial concentration of TEOS is higher than the one required to obtain the stoichiometry, XRD diagrams show only a poorly crystallized clinoenstatite phase (figure 3.a).

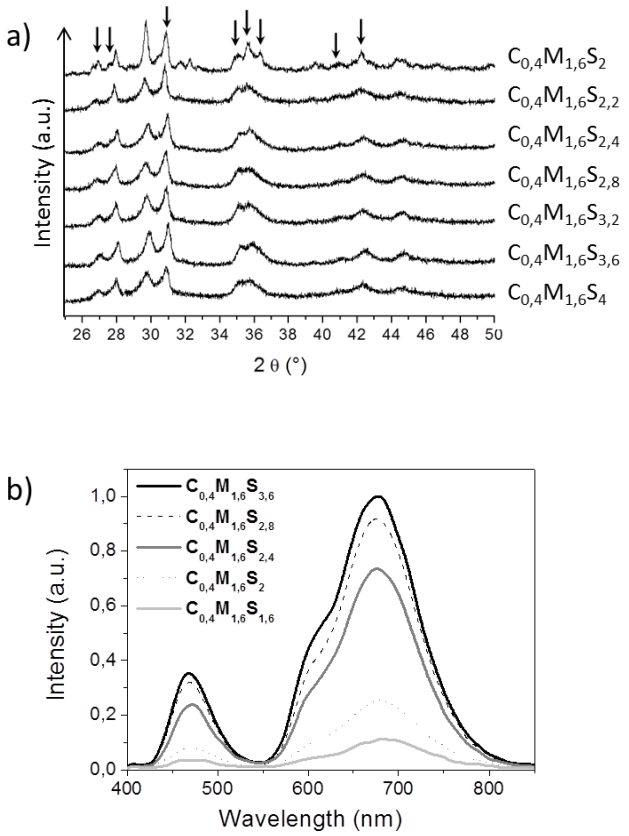

Figure 3. (a) XRD patterns of serie B with various silica contents (arrows point out diopside phase) and (b) corresponding LLP spectra.

However, when the initial concentration of silica is just enough to obtain pyroxene phase (C0.4M1.6S2), XRD diagram shows also the presence of diopside phase. For this silicate, 30% additional calcium in the Mg2Si2O6 initial formula are sufficient to obtain the two phases: clinoenstatite and diopside as previously reported [30]. With the increase of silica content, the nucleation of clinoenstatite can be explained considering the better diffusion of Mg2+ ions inside the silica glass during the thermal crystallization compared to bigger Ca2+ ions which probably remain trapped in the silica matrix. For lower silica content, the proximity of Ca2+ and Mg2+ ions in the matrix promotes the crystallization of the diopside

phase, since the ions diffusion distance for the nucleation of this phase is shorter. Persistent luminescence spectra of series B (figure 3.b) showed the same three characteristic emission bands (480 nm, 580 nm, 680 nm) than for A serie. When the initial concentration of silicon is higher than the one required to obtain the stoichiometry, persistent luminescence intensity increases due to better crystallinity of compound. This suggests that thermal treatment need to be optimized for the different concentrations.

Such study has been done for the Ca0.3Mg1.7Si3O8 doped (C2 composition). After drying at 90°C for 30h, samples were annealed from 900°C to 1400°C for 10 h under reductive atmosphere. XRD (figure 4.a) show that diopside phase is obtained for a thermal treatment at 1150°C, an annealing temperature higher than the one required for the first generation of compounds [24]. This result well agrees with a higher initial concentration of TEOS and a more limited diffusion of ions. At this temperature, the amorphous silica ratio, deduced from 29Si quantitative NMR spectra, is the lowest, agreeing with a better crystallization of the compound (table 1). Since the particle size depends on thermal treatment temperature, the NPs size was determined here by Debye-Scherrer method. An increase of the size with the increase of the temperature was previously observed [24]. This increase was not observed when the nanoparticles are synthetized by a sol-gel method inspired by Stöber process (table 1).

Table 1. Amorphous silica ratio of $Ca_{0.3}Mg_{1.7}Si_3O_8$: Eu1%Mn5%Dy2% compound depend on thermal treatment temperature. Amorphous and crystalline silica contents have been deduced from integration of NMR peaks between -210 ppm and -120 ppm and between -70ppm and -95 ppm respectively. Particle sizes have been deduced from XRD patterns using Debye-Scherrer method.

Thermal treatment temperature	Amorphous silica content	Crystallized silica content	Nanoparticle size (nm)
900°C	48.1%	51.9 %	50
1050°C	41.6%	58.4%	53
1150°C	23%	77%	51

The particles have 50 nm in diameter whatever the thermal treatment temperature in the range of 900-1150°C. This is probably related to the presence of amorphous silica shell which prevents the sintering of nanoparticles. According to the crystallization degree, the sample annealed at 900°C is not persistent whereas the one annealed at 1150°C exhibit more intense emission and persistent luminescence (Figure 4.b). The persistent luminescence spectrum for Ca0.3Mg1.7Si3O8: Eu1% Mn5% Dy2% shows only emission from one crystallographic site Mn2+Mg, leading to an emission centered at 680 nm. This point is very important as we aim to develop red/near infrared nanosensors for bioimaging applications.

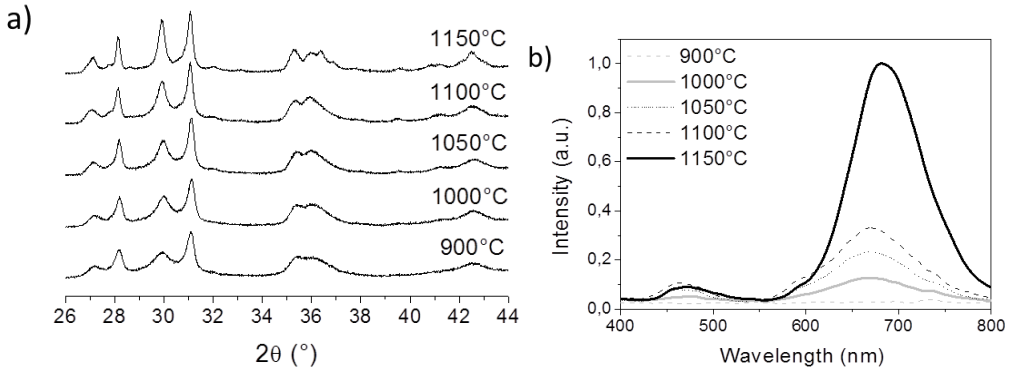

Figure 4. (a) XRD patterns and (b) LLp spectra of C0.3M1.7S3O8: Eu1% Mn5% Dy2% compound depending on thermal treatment temperature

Post annealing treatments. After thermal treatment, the nanoparticles obtained by sol-gel synthesis inspired by Stöber process are coated by a layer of amorphous silica and strongly aggregated. The samples need to be treated in order to reduce the thickness of the amorphous silica coating. Several treatments were investigated using different leaching agents such as NaOH, 2M, NH4F, 10M and NH5F2, 0.5M. Samples are put in an aqueous solution of NaOH 2M, NH4F 10M or NH5F2 0.5M and stirred at room temperature for 2 hours with NaOH, and 1 h for the case of NH4F or NH5F2. The product is then thoroughly washed and dried under air. XRD diagrams show no phase modification after such leaching treatments (figure 5.a) and the crystalline particle size is unmodified for NaOH and NH5F2 reactants. However, for leaching with NH4F 10M, there are additional new peaks on the pattern corresponding to CaF2 and MgF2 phases. This means that this treatment is too strong and destructive and leads to both silica shell and crystalline core dissolution. The sample which present the closest crystallization to the raw material is the sample treated with NH5F2 0.5M. This treatment seems to be less aggressive for the silicate nanoparticles.

As can be seen on the TEM images of figure 6, a thick layer of amorphous silica is still visible for the sample treated with NaOH 2M (see table 2). This decrease of the amount of silica is confirmed by EDX analysis while the Ca / Mg ratio remains the same (see table S.I.1). With NH4F 10 M, spherical nanoparticles coated by a less thick layer of amorphous silica are obtained. The amorphous coating is the thinnest after a treatment of the sample with NH5F2 0.5M. Spherical and monodisperse nanoparticles coated by a layer of amorphous silica of 2.7 nm are then obtained.

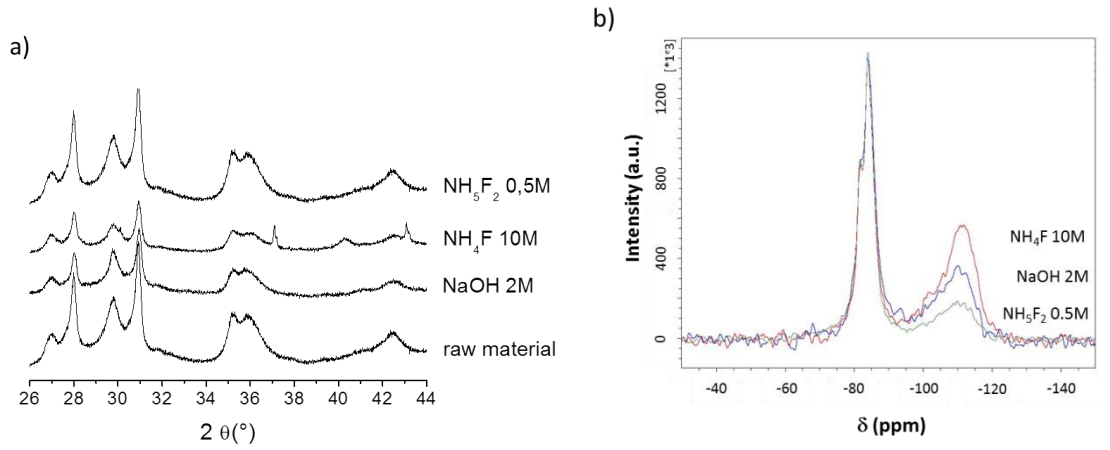

Figure 5. (a) XRD patterns and (b) NMR 29Si spectra of C0.3M1.7S3O8: Eu1% Mn5% Dy2% composition (T = 1150°C) as raw material and depending on post-annealing treatment: NaOH 2M, NH4F 10M and NH5F2 0.5M.

Table 2. Thickness of amorphous silica layer depending on post-annealing treatment: NaOH 2M, NH_4F 10M and NH_5F_2 0.5M. Content of silica shell compared to total silicon.

Post-annealing treatment	Thickness of amorphous silica shell	Amorphous silica ratio	Total silicon ratio
As prepared	/	/	30.0%
NaOH 2M	20 nm	37.3%	29.3%
NH_4F 10M	16 nm	47%	26.8%
NH_5F_2 0.5M	2.7 nm	22%	24.7%

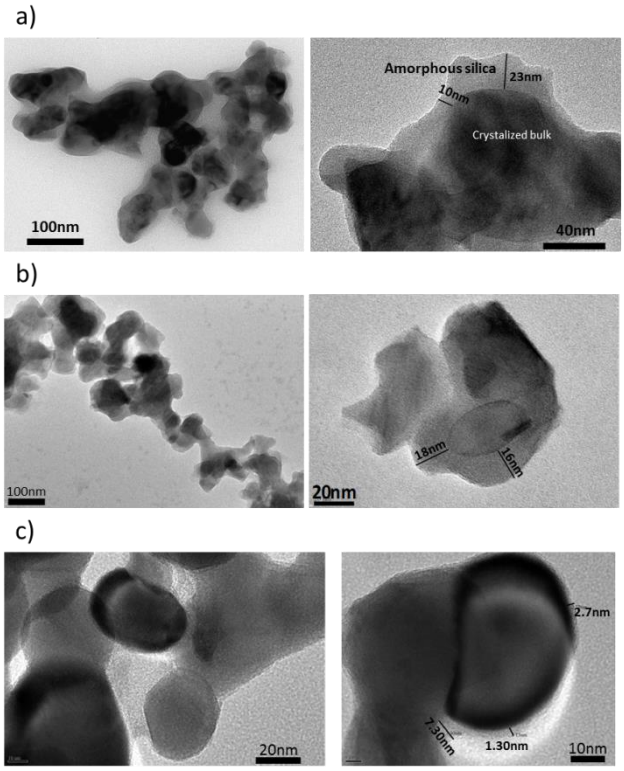

Figure 6. TEM images of C0.3M1.7S3O8: Eu1% Mn5% Dy2% compound depending on post-annealing treatment: (a) NaOH 2M, (b) NH4F 10M and (c) NH5F2 0.5M.

NMR 29Si spectra of etched samples (figure 5.b) show two different domains: a peak from -80 to -95 ppm corresponding to crystalline silicate and a larger peak from -100 to -120 ppm corresponding to amorphous silica. NMR experiments confirm that the sample treated with NH5F2 0.5M contains the lowest amount of amorphous silica as the second peak is less intense for that sample. A fundamental chemical analysis confirmed that the sample treated with NH5F2 0.5M indeed contains less silicon (table 2). The treatment with NH5F2 0.5M seems to be really the most efficient treatment and produces spherical silicates nanoparticles coated by a thin (2.7 nm) layer of amorphous silica without any change on chemical composition of crystalline core (table S.I.1). The homogeneity of both chemical composition and grain size of as treated particles is effective as reported in supplementary information (table S.I.2 and figure S.I.1). EDX analysis on small zones noted the low variability in chemical composition from zone to zone (< 2% of variability) and that the resulting mean composition is in very good accordance with that of larger zone. In addition, SEM images show regular and homogeneous grain size for both as-prepared and treated sample suggesting that the step of silica dissolution did not affect crystalline particles.

The yield of usable small nanoparticles for in vivo optical imaging after etching increased from 15% for a treatment with NaOH 2M up to 65% for a treatment with NH5F2 0.5M. Therefore a great improvement was made in terms of silica etching to obtain small nanoparticles with satisfactory persistent luminescence properties. This lead to a better dispersion of nanoparticles in suspension as reported to figure S.I.2. The persistent luminescence spectra and persistent decay curves within 30 min of Ca0.3Mg1.7Si3O8: Eu1% Mn5% Dy2% compound (figure 7) shows that persistent luminescence is more intense for the raw material before etching.

This could be attributed to some surface effects when the layer of amorphous silica is thinner and almost removed. Indeed silica layer play a protective role preventing surface related non-radiative phenomena. Comparing the surface treatments, it appears that the sample treated with NH5F2 0.5M is the most luminescent and persistent whereas the sample treated with NH4F 10M exhibits less intense persistent luminescence. The surface treatment with NH5F2 0.5M indeed is the most efficient treatment because it reduces the aggregation of the NPs, produces spherical silicates nanoparticles coated by a thin layer of amorphous silica that still have good persistent luminescence properties.

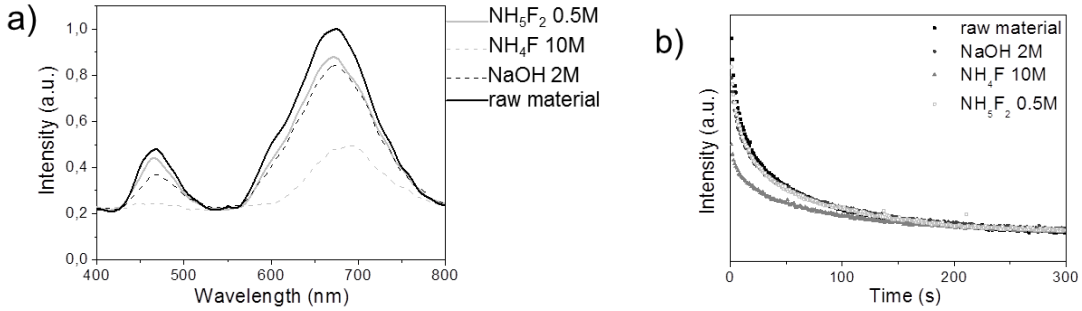

Figure 7. (a) Persistent luminescence spectra of C0.3M1.7S3O9: Eu1% Mn5% Dy2% depending on post-annealing treatment: NaOH 2M, NH4F 10M and NH5F2 0.5M and (b) luminescence decay curves (λexc = 365 nm – texc = 120s).

Conclusions

CaxMgySi2O6 doped Eu2+, Mn2+, Dy3+ nanoparticles were prepared by a sol–gel method inspired by Stöber process in order to develop red-near infrared persistent luminescence

nanoparticles as sensors for optical imaging. In the aim of improving the persistent luminescence and studying the chemical composition influence on the persistent luminescence properties, materials with various Ca/Mg/Si molar ratio have been prepared. Composition that favors the enstatite structure with good distribution of Mn2+ into the two coordinated sites of this structure exhibits an enhancement of long lasting phosphorescence in red-near infrared range. Crystallinity can also be optimized adjusting temperature of heating treatment. Nanoparticles with 50 nm size were treated in NH5F2 0.5M aqueous solution after thermal treatment in order to reduce the thickness of the amorphous silica coating. Ca0.3Mg1.7Si3O8 doped Eu2+ (1%), Mn2+ (5%), Dy3+ (2%) non aggregated nanoparticles with a thin silica layer (2.7 nm) and very promising optical properties at 680 nm were successfully obtained. Such nanoparticles are relevant as nanoprobes for in vivo optical imaging and diagnostics applications.

Experimental Section

All chemicals of analytic grade reagents were used without further purification

Synthesis of long lasting luminescent nanoparticles. Two different solutions were prepared: the first one SA is obtained by mixing absolute ethanol (92mL), water (14mL) and ammoniac solution (30% - 6mL), and the second one, SB, by dissolution of matrix precursors, Mg(NO3),2.6H2O, CaCl2, and tetraethyl orthosilicate (TEOS) with doping precursors, MnCl2, EuCl3.6H2O and Dy(NO3)3.5H2O in 8ml of absolute ethanol. SB is added to SA drop by drop under vigorous stirring at room temperature. The obtained sol was stirred at room temperature for 24h, then dried at 90°C for 30h, and annealed at high temperature (1050-1150°C) for 10h under reductive atmosphere (95% N2, 5% H2). This last step is crucial to reduce Eu3+ in Eu2+, allowing the persistent luminescence properties.

Three main sample series have been prepared. The series A is consisting on various Ca/Mg ratios from CaMgSi2O6 labelled C1M1S2, to Ca0.3Mg1.7Si2O6 labelled C0.3M1.7S2. The content in silica was varied in series B, with a ratio Ca/Mg=0.22, from pyroxene based stoichiometric silica content (C0.4M1.6S2) to an excess in silica content (C0.4M1.6S4). Both these series, A and B, contain the same doping rate namely Eu2+(0.5%), Mn2+(2.5%), Dy3+(1%) labelled “doped C1”. In another series C, the content of doping ions has been increased by two for two different chemical compositions: Ca0.5Mg1.5Si2O6: Eu1% Mn5% Dy2% (C0.5M1.5S2 doped C2) and Ca0.6Mg1.4Si2O6: Eu1% Mn5% Dy2% (C0.6M1.4S2 doped C2).

Silica leaching. As obtained PLNPs are coated by a layer of amorphous silica and are strongly aggregated. Samples have been thus treated in order to reduce the thickness of the amorphous silica coating using the following procedure. PLNPs powder is added in an aqueous solution of NaOH 2M, NH4F 10M or NH5F2 0.5M and stirred at room temperature for 24h with NaOH and 1h for NH4F and NH5F2. The product is then thoroughly washed with distilled water and dried under air flux. Structural and optical characterizations. Powder X-ray diffraction (XRD) study was performed on a Bruker D8 Advance diffractometer using Cu-Kα1,α2 radiation (λ = 1.5418 Å) at 45 kV and 40 mA, 0.0046°θ step size and 0.5s step time over a range of 10°2θ to 80°2θ. Transmission electron microscopy (TEM) images were acquired with a FEI Tecnai 120 Twin microscope operating at 120 kV and equipped with a high resolution Gatan Orius CCD 4 k 64 k numeric camera. Excitation and emission spectra were measured on powdered samples with a Varian Cary Eclipse Fluorescence spectrophotometer at room temperature. Long lasting phosphorescence (LLP) spectra were recorded after 2 minutes irradiation with UV light, and the resulting signal was collected via an optical fiber by Roper Scientific Pixis 100 CCD camera cooled at -68°C coupled with an Acton SpectraPro 2150i spectrometer for spectral analysis. The resolution of the emission is about 10 nm ($\Delta\lambda$/a = 10 nm/mm) according to the experimental spectrophotometer (f=125mm, 300tr/mm blazed at 500nm). In order to compare the LLP spectra, a normalization of their intensities was done systematically. Electron paramagnetic resonance (EPR) measurements were performed with a Bruker Elexsys E500 spectrometer equipped with a Super-High-Q cavity and working at a microwave frequency of 9.4 GHz. The spectra were recorded at room temperature with a microwave power of 2 mW and a modulation field of 1 mT.

Silica shell dissolution has been studied using solid state 29Si Nuclear Magnetic Resonance (NMR). Spectra were recorded with a standard 7 mm double resonance probe on a 7 T Bruker Avance III spectrometer operating at 300 MHz for 1H and 59 MHz for 29Si. Spinning speed was set to 5 kHz and sample was packed into a 7 mm zirconia rotor. The used pulse sequence was a single 1.5 µs π/6 pulse with 45 kHz 1H decoupling during acquisition. A relaxation delay of 60 s was applied without decoupling.

Acknowledgements

This work was supported by the French National Research Agency (ANR) in the frame of its Nanosciences and Nanotechnologies program (NATLURIM-ANR-08-NANO-025).

Keywords: Diopside silicate, nanoprobes, Persistent luminescence, Long Lasting Phosphorescence, Optical Imaging

[1] J.V. Frangioni, Curr. Opin. Chem. Biol. 2003, 7, 626-634.

[2] W.F. Cheong, S.A. Prahl, A.J. Welch, IEEE J. Quantum Electron. 1990, 26, 2166-2185.

[3] A.P. Castano, T.N. Demidova, M.R. Hamblin, Photodiagnosis and Photodynamic Therapy 2004, 1, 279-293.

[4] A. C. B. Murray, C. R. Kagan, Annu. Rev. Mater. Sci. 2000, 30, 545-610.

[5] E. Cassette, M. Helle, L. Bezdetnaya, F. Marchal, B. Dubertret, T. Pons, Adv. Drug Delivery Rev. 2013, 65, 719-731.

[6] Y. Luab, W. Chen, Chem. Soc. Rev., 2012, 41, 3594–3623.

[7] F. Grasset, F. Dorson, S. Cordier, Y. Molard, C. Perrin, A.M. Marie, T. Sasaki, H. Haneda, Y. Bando, M. Mortier, Adv. Mater. 2008, 20, 143–148.

[8] S. Cordier, Y. Molard, K. A. Brylev, Y.V. Mironov, F. Grasset, B. Fabre, N. G. Naumov, J. Clust. Sci., 2015, 26, 53–81.

[9] T. Matsuzawa, Y. Aoki, N. Takeuchi, Y. Murayama, J. Electrochem. Soc. 1996, 143, 2670-2673.

[10] T. Katsumata, T. Nabae, K. Sasajima, T. Matsuzawa, J. Cryst. Growth 1998, 183, 361-365.

[11] D. Jia, R.S. Meltzer, W.M. Yen, W. Jia, X.J. Wang, Appl.Phys. Lett. 2002, 80, 1535-1537.

[12] N. Kodama, T. Takahashi, M. Yamaga, Y. Tanii, J. Qiu, K. Hirao, Appl. Phys. Lett. 1999, 75, 1715-1717.

[13] J.-C.G. Bunzli, S.V. Eliseeva, J. of Rare Earths 2010, 2, 824-842.

[14] X. Wang, D. Jia, W.M. Yen, J. Lumin. 2003, 102-103, 34-37.

[15] Jin, Hu, Chen, Wang, Mu, Ju, Wang, Mater. Lett. 2014, 126, 75-77.

[16] Sun, Jia, Zhao, Li, Fu, Jiang, Zhang, Pang, Li, Opt. Mater. 2014, 36, 1841-1845.

[17] G. Zhu, Chen, Ge, J. Mater. Sci. Mater. Electron 2014, 25, 2857-2862.

[18] T. Maldiney, B. Viana, A. Bessiere, D. Gourier, M. Bessodes, D. Scherman, C. Richard, Opt. Mater. 2013, 35, 1852-1858.

[19] T. Maldiney, A. Bessière, J. Seguin, E. Teston, S. K. Sharma, B. Viana, A. J.J. Bos, P. Dorenbos, M. Bessodes, D. Gourier, D. Scherman, C. Richard. Nat. Mater. 2014, 13, 418-426

[20] T. Maldiney, G. Sraiki, B. Viana, D. Gourier, C. Richard, D. Scherman, M. Bessodes,. K. Van den Eeckhout, D. Poelman, P.F. Smet, Opt. Mater. 2012, 2, 261-268

[21] G. Mialon, M. Gohin, T. Gacoin, J-P. Boilot, ACS Nano 2012, 2, 2505-2512.

[22] Z.J. Li, J.P. Shi, H.W. Zhang, M. Sun, Opt. Express 2014, 22, 10509-10518.

[23] Y.-J. Chuang, Z. Zhen, F. Zhang, F. Liu, J. P. Mishra, W. Tang, H. Chen, X. Huang, L. Wang, X. Chen, J. Xie, Z. Pan, Theranostics 2014, 4, 1112-1122.

[24] N. Q. Le Masne de Chermont, C. Chanéac, J. Seguin, F. Pellé, S. Maitrejean, J-P Jolivet, D. Gourier, M. Bessodes, D. Scherman, Proc. Natl. Acad. Sci. USA 2007, 104, 9266-9271.

[25] X. Wang, D. Jia, W.M. Yen, J. Lumin. 2003, 102-103, 34-37.

[26] T. Maldiney, A. Lecointre, B. Viana, A. Bessiere, M. Bessodes, D. Gourier, C. Richard, D. Scherman, J. Am. Chem. Soc. 2011, 133, 11810-11815.

[27] A. Bessiere, A. Lecointre, K.R. Priolkar, D.Gourier, J. of Mater. Chem. 2012, 22, 19039-19046.

[28] C. Rosticher, C. Chaneac, B. Viana, A. Bessiere, J. Lumin. 2012, 27, 157-158.

[29] W.L. Brown, N. Morimoto, J.V. Smith, J. Geology. 1961, 69, 609-616.

[30] A.J. Poldervaart, H.H. Hess, J. Geology.1951, 59, 472-489.

[31] R.D. Shannon, C.T. Prewitt, Acta Crystallogr. 1969, 25, 925-946.

[32] A. Lecointre, A. Bessière, B. Viana, D. Gourier, Rad. Measurements 2010, 45, 497-499.

[33] A. Lecointre, A. Bessiere, K. R. Priolkar, Mater. Res. Bull. 2013, 48, 1898-1905.

[34] Y. Zhuang, Y. Katayama, J. Ueda, S. Tanabe, Opt. Mater. 2014, 36, 1907-1912.

Supplementary Information

New insight out $CaMgSi_2O_6:Eu^{2+}$, Mn^{2+}, Dy^{3+} nanoprobes: Influence of chemical composition and crystallinity on persistent red luminescence

Céline Rosticher,[1] Bruno Viana,[2] Guillaume Laurent,[1] Patrick Le Griel,[1] Corinne Chanéac,*[1]

[a] C. Rosticher, G. Laurent, P. Le Griel, C. Chanéac
Sorbonne Universités, UPMC Univ Paris 06, CNRS, Collège de France, Laboratoire de Chimie de la Matière Condensée de Paris, 11 place Marcelin Berthelot, 75005 Paris, France.
E-mail: corinne.chaneac@upmc.fr

[b] B. Viana,
PSL Research University, Chimie ParisTech - CNRS, Institut de Recherche de Chimie Paris, 11 rue Pierre et Marie Curie, 75005 Paris, France

Relative atomic %	% Si	% Ca	% Mg
Nominal composition	60	6	34
As prepared sample: Experimental composition from EDX	62.2	4.1	33.7
As prepared sample: Experimental composition from ICP	62.1	5.6	32.3
After silica leaching: Experimental composition from EDX	56.1	5.8	38.1
After silica leaching: Experimental composition from ICP	54.2	6.8	39.0

Table S.I. 1. Comparison of chemical composition for as prepared sample and after silica leaching using NH_5F_2. These results are given for $Ca_{0.3}Mg_{1.7}Si_3O_8$: Eu^{2+} 1%, Mn^{2+} 5%, Dy^{3+} 2% compound.

Relative atom. %	**SZ1**	**SZ2**	**SZ3**	**SZ4**	**SZ5**	**SZ6**	**SZ7**	**SZ8**	**SZ9**	**SZ10**	**Mean SZ**	**LZ 1**	**LZ 2**
Si	56.0	56.2	56.9	56.6	57.2	57.6	56.9	56.3	56.8	56.8	56.7	55.9	56.3
Ca	5.8	5.5	5.8	5.5	5.4	5.0	5.7	5.6	5.6	5.9	5.6	5.9	5.7
Mg	38.2	38.4	37.3	37.9	37.4	37.4	37.4	38.1	37.6	37.3	37.7	38.2	38.0

Table S.I. 2. Study of the homogeneity of chemical composition of $Ca_{0.3}Mg_{1.7}Si_3O_8$: Eu^{2+} 1%, Mn^{2+} 5%, Dy^{3+} 2% compound using NH_5F_2, deduced from EDX analysis on ten small zones, *SZ*, (mapping mode: local chemical composition on 500nm x 500nm surface) and on two larger zones, *LZ*, (average chemical composition on 30µm x 30µm surface).

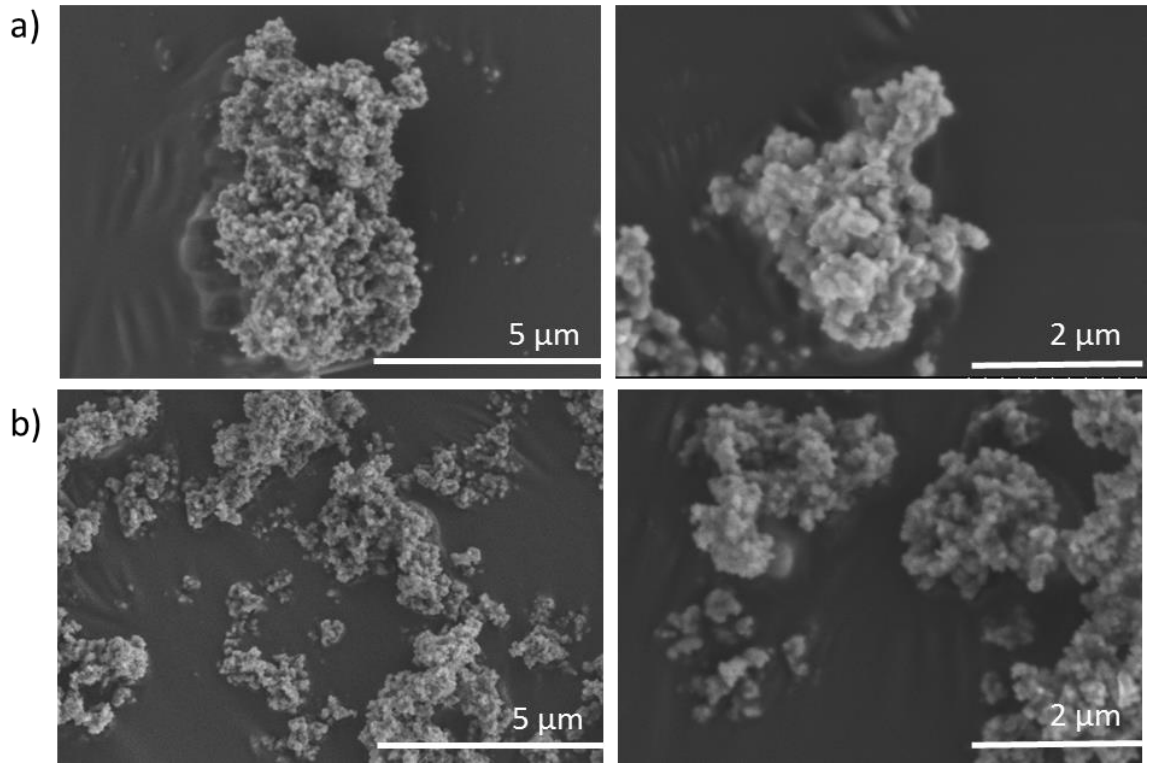

Figure S.I. 1 : SEM images of $Ca_{0.3}\,Mg_{1.7}\,Si_3O_8$: Eu^{2+} 1%, Mn^{2+} 5%, Dy^{3+} 2% compound before and after silica leaching using NH_5F_2. SEM has been performed on Hitachi S-3400N equipped of EDX spectrometer (Oxford Instruments - X-max).

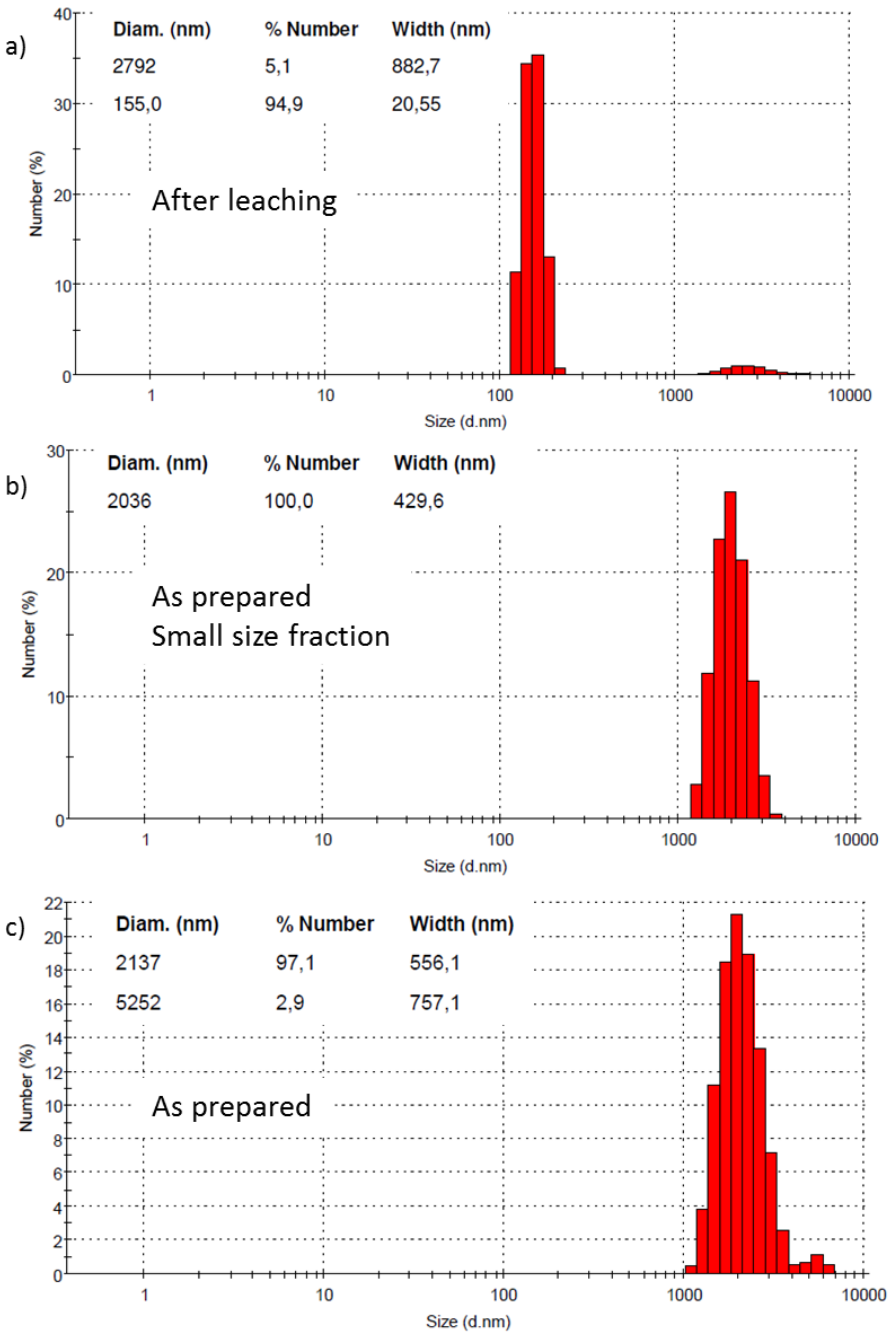

Figure S.I. 2 : Size distribution of $Ca_{0.3}Mg_{1.7}Si_3O_8$: Eu^{2+} 1%, Mn^{2+} 5%, Dy^{3+} 2% compound dispersed in water (1mg/mL). Distribution of (a) nanoparticles suspension after silica leaching, (b) supernatant obtained after 2 hours of sedimentation of as-prepared nanoparticles, and (c) crude suspension of as-prepared nanoparticles. Suspension of nanoparticles is prepared following a first step of peptisation (2 hours in NaOH 1M), a centrifugation of nanoparticle and their dispersion in pure water.